The effects of degraded spatial coherence on ultrafast-laser channel etching

Jesse Dean,[1] **Martin Bercx,**[1] **Felix Frank,**[1] **Rodger Evans,**[1,3] **Santiago Camacho-López,**[1,3] **Marc Nantel**[1,2] **and Robin Marjoribanks**[1]

[1]*Dept. of Physics and Institute for Optical Sciences, University of Toronto, 60 St George St., Toronto ON, M5S 1A7, Canada*

[2]*Centre for Photonics, Ontario Centres of Excellence, Inc. Suite 250, 2655 North Sheridan Way, Mississauga, ON, L5K 2P8*

[3]*Present address: Centro de Investigación Científica y de Educación Superior de Ensenada, Km 107 Carretera Tijuana-Ensenada, Ensenada, Baja California 22860, Mexico*

jdean@physics.utoronto.ca

Abstract: When laser-etching channels through solid targets, the etch-rate is known to decrease with increasing depth, partly because of absorption at the sides of the channel. For ultrafast-laser pulses at repetition rates >100MHz, we show that the etch-rate is also affected by optical properties of the beam: the channel acts as a waveguide, and so the pulses will decompose into dispersive normal modes. Additionally, plasma on the inner surface of the channel will cause scattering of the beam. These effects will cause a loss of spatial coherence in the pulse, which will affect the propagated intensity distribution and ultimately the etch-rate. We have characterized this effect for various foil thicknesses to determine the evolution of the beam while drilling through metal.

OCIS codes: (350.3850) Materials processing; (030.1640) Coherence; (350.5400) Plasmas; (080.1510) Propagation methods.

References and links

1. X. Liu, D. Du, and G. Mourou, "Laser ablation and micromachining with ultrashort laser pulses," IEEE J. Quantum Electron. **33**, 1706–1716 (1997).
2. P. P. Pronko, P. A. VanRompay, C. Horvath, F. Loesel, T. Juhasz, X. Liu, and G. Mourou, "Avalanche ionization and dielectric breakdown in silicon with ultrafast laser pulses," Phys. Rev. B **58**, 2387–2390 (1998).
3. S. Camacho-Lopez, R. Evans, C. Greenhalgh, C. Torti, J. Robertson, R. Marjoribanks, P. Herman, M. Nantel, and L. Lilge, "Single-pulse and 'pulsetrain-burst' (>100 MHz) effects in ultrafast laser processing of metals, glasses, and bio-tissues," in *Technical Digest, Conference on Lasers and Electro-Optics (CLEO), 2003 (Optical Society of America, Baltimore, MD, USA), TOPS* (2003).
4. S. Nolte, G. Kamlage, R. Korte, T. Bauer, T. Wagner, A. Ostendorf, C. Fallnich, and H. Welling, "Microstructuring with femtosecond lasers," Advanced Engineering Materials **2**, 23–27 (2000).
5. H. Zheng, E. Gan, and G. C. Lim, "Investigation of laser via formation technology for the manufacturing of high density substrates," Opt. Lasers Eng. **36**, 355–371 (2001).
6. J. Neev, L. Da Silva, M. Feit, M. Perry, A. Rubenchik, and B. Stuart, "Ultrashort pulse lasers for hard tissue ablation," IEEE J. Sel. Top. Quantum Electron. **2**, 790–800 (1996).
7. F. H. Loesel, J. P. Fischer, M. H. Götz, C. Horvath, T. Juhasz, F. Noack, N. Suhm, and J. F. Bille, "Non-thermal ablation of neural tissue with femtosecond laser pulses," Appl. Phys. B **66**, 121–128 (1998).
8. T. Juhasz, F. Loesel, R. Kurtz, C. Horvath, J. Bille, and G. Mourou, "Corneal refractive surgery with femtosecond lasers," IEEE J. Sel. Top. Quantum Electron. **5**, 902–910 (1999).
9. S. Preuss, A. Demchuk, and M. Stuke, "Sub-picosecond UV laser ablation of metals," Appl. Phys. A **61**, 33–37 (1995).

#96527 - $15.00 USD Received 3 Jun 2008; revised 30 Jul 2008; accepted 17 Aug 2008; published 20 Aug 2008

10. C. Momma, B. N. Chichkov, S. Nolte, F. von Alvensleben, A. Tünnermann, H. Welling, and B. Wellegehausen, "Short-pulse laser ablation of solid targets," Opt. Commun. **129**, 134–142 (1996).
11. S. Nolte, C. Momma, H. Jacobs, A. Tünnermann, B. N. Chichkov, B. Wellegehausen, and H. Welling, "Ablation of metals by ultrashort laser pulses," J. Opt. Soc. Am. B **14**, 2716–2722 (1997).
12. H. Varel, D. Ashkenasi, A. Rosenfeld, M. Wähmer, and E. E. B. Campbell, "Micromachining of quartz with ultrashort laser pulses," Appl. Phys. A **65**, 367–373 (1997).
13. L. Shah, J. Tawney, M. Richardson, and K. Richardson, "Femtosecond laser deep hole drilling of silicate glasses in air," Appl. Surf. Sci. **183**, 151–164 (2001).
14. M. Lapczyna, K. P. Chen, P. R. Herman, H. W. Tan, and R. S. Marjoribanks, "Ultra high repetition rate (133 MHz) laser ablation of aluminum with 1.2-ps pulses," Appl. Phys. A **69**, 883–886 (1999).
15. P. R. Herman, A. Oettl, K. P. Chen, and R. S. Marjoribanks, "Laser micromachining of transparent fused silica with 1-ps pulses and pulse trains," in *Commercial and Biomedical Applications of Ultrafast Lasers*, M. K. Reed and J. Neev, eds., pp. 148–155 (1999).
16. R. Marjoribanks, Y. Kerachian, P. Herman, S. Camacho-Lopez, and M. Nantel, "Pulsetrain 'burst' machining: ultrafast-laser microprocessing at ultrahigh (>100 MHz) pulse-rates," in *Technical Digest, Conference on Lasers and Electro-Optics (CLEO), 2001 (Optical Society of America, Baltimore, MD, USA), TOPS Vol. 56* (2001).
17. D. Breitling, D. Fohl, F. Dausinger, T. Kononenko, and V. Konov, "Drilling of metals," in *Femtosecond Technology for Technical and Medical Applications*, vol. 96 of *Topics in Applied Physics*, pp. 131–156 (Springer Berlin / Heidelberg, 2004).
18. A. M. Komashko, M. D. Feit, A. M. Rubenchik, M. D. Perry, and P. S. Banks, "Simulation of material removal efficiency with ultrashort laser pulses," Appl. Phys. A **69**, 95–98 (1999).
19. S. R. Franklin and R. K. Thareja, "Simplified model to account for dependence of ablation parameters on temperature and phase of the ablated material," Appl. Surf. Sci. **222**, 293–306 (2004).
20. B.-M. Kim, M. D. Feit, A. M. Rubenchik, E. J. Joslin, P. M. Celliers, J. Eichler, and L. B. D. Silva, "Influence of pulse duration on ultrashort laser pulse ablation of biological tissues," J. Biomed. Opt. **6**(3), 332–338 (2001).
21. A. E. Wynne and B. C. Stuart, "Rate dependence of short-pulse laser ablation of metals in air and vacuum," Appl. Phys. A **76**, 373–378 (2003).
22. R. S. Marjoribanks, F. W. Budnik, L. Zhao, G. Kulcsar, M. Stanier, and J. Mihaychuk, "High-contrast terawatt chirped-pulse-amplification laser that uses a 1-ps Nd:glass oscillator," Opt. Lett. **18**, 361–363 (1993).
23. J. Dean, M. Bercx, M. Nantel, and R. Marjoribanks, "Transverse coherence measurement using a folded Michelson interferometer," J. Opt. Soc. Am. A **24**, 1742–1746 (2007).
24. L. Mandel and E. Wolf, *Optical Coherence and Quantum Optics*, chap. 5, pp. 252–287 (Cambridge University Press, 1995).
25. Z. Guosheng, P. M. Fauchet, and A. E. Siegman, "Growth of spontaneous periodic surface structures on solids during laser illumination," Phys. Rev. B **26**(10), 5366–5381 (1982).
26. J. F. Young, J. S. Preston, H. M. van Driel, and J. E. Sipe, "Laser-induced periodic surface structure. II. Experiments on Ge, Si, Al, and brass," Phys. Rev. B **27**(2), 1155–1172 (1983).
27. C. S. Nielsen and P. Balling, "Deep drilling of metals with ultrashort laser pulses: A two-stage process," J. Appl. Phys. **99**(9), 093101 (2006).

1. Introduction

From the time the laser became a "solution in search of a problem", one of the earliest problems for it to address well is to drill holes in materials where mechanical methods were not well suited. Lasers have proved very effective for etching tiny channels, especially those with high aspect-ratios, and ultrashort (*i.e.*, subpicosecond) pulses —with their qualitatively different heat-deposition effects and stable etch-threshold behaviour —have recently been shown to offer striking improvements for certain materials[1, 2, 3].

Ultrashort-pulse lasers allow precise machining of a variety of materials including transparent dielectrics, metals, and organic tissues. These have multiple applications in materials microstructuring, nanotechnology and medicine[4]; they can provide enabling technologies, for example microscopic vias in lithographic circuitry[5]. Where conventional drilling becomes expensive, such as for high-aspect-ratio holes where drill-bits frequently break, ultrashort-pulse laser-drilling can improve manufacturing yield and performance parameters. Beyond manufacturing, ultrashort-pulse lasers have been found to be useful for processing hard[6] and soft[7] biological tissue. In particular, ultrashort-pulse lasers allow clean incisions with minimized collateral thermal impact —an especially important issue in laser eye-surgery[8].

#96527 - $15.00 USD Received 3 Jun 2008; revised 30 Jul 2008; accepted 17 Aug 2008; published 20 Aug 2008

Previous studies have investigated how various characteristics of the beam (such as pulse duration, number of pulses, intensity, *etc.*) affect the nature of the channel being etched (*e.g.*, depth and diameter) [9, 10, 11, 12, 13]. Pulsetrain-burst processing, which uses a short series of ultrashort pulses at a repetition rate of 1 MHz or greater, has been shown to greatly reduce shock damage and cracking in glass and brittle materials, and to produce a cleaner, smoother surface [14, 15, 16], but relatively little is known of the impact of this high-repetition-rate approach for laser channel-etching.

In general, the per-pulse etch-rate drops nearly exponentially with depth (Fig. 1); Breitling *et. al* have characterized this at modest repetition-rates for metal targets [17]. This significantly limits the laser-cut depth of high-aspect-ratio holes —a better understanding of this reduction could guide us to a way to eliminate the problem or mitigate it. The slight taper typical of laser-etched channels can produce back-reflection, but the main causes for decreased etch rates have been assumed to be related to absorption of the light at the channel sidewalls. The process of absorption is quite complicated: the effects of varying pulse duration, fluence, angle of incidence, polarization, prepulse, and material temperature have been studied through theoretical modeling[18, 19]; the influence of the pulse length, fluence, hole depth, and ambient pressure on etch parameters have been characterized experimentally as well[20, 21].

Although there has been extensive research on how the etched channel depends on various laser parameters, there has been relatively little direct investigation into how the laser pulse may be optically altered by the boundary conditions imposed by the channel. In particular, little is known about how the optical-phase properties of the laser pulses may change while propagating, and how this might contribute optically to the reduction of the etch-rate. Loss of temporal or spatial coherence, and group-velocity dispersion, could each contribute to a decreased etch-rate.

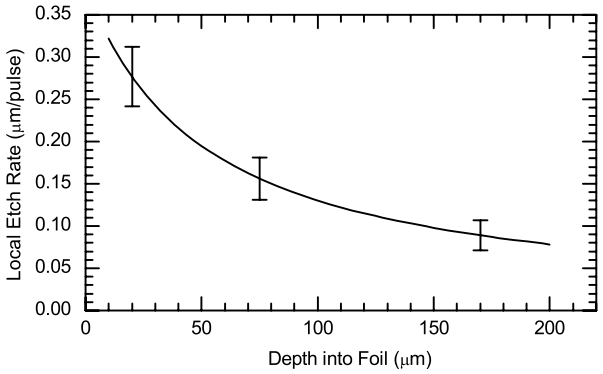

Fig. 1. Observed etch rate, per pulse, differentially localized to different depths in aluminum foil, for 133MHz pulsetrains of 1ps pulses as described in experimental setup.

A channel, as it is being drilled, may be approximated as a cylindrical waveguide. In our experiments with repetition rates of 133MHz, waveguiding is demonstrated clearly, in that the image of the beam at the exit of the channel being drilled is quite different from the image of a freely-propagated beam at the same plane (Fig. 2). The Gaussian beam propagated through the cylindrical channel will analyze over the normal modes (Bessel functions), which are dispersive. This dispersion will change optical-phase relationships: the pulse will stretch, and the intensity pattern may develop intermediate-field interference structures. Channel asymmetries, surface roughness and plasma formed on the inner surface of the channel may further complicate the boundary conditions. Of particular interest to us, refraction and scattering, includ-

#96527 - $15.00 USD Received 3 Jun 2008; revised 30 Jul 2008; accepted 17 Aug 2008; published 20 Aug 2008

ing phase shifts associated with plasma coupling, may degrade the spatial coherence of the etching-pulse. This would in turn lead to redistribution of energy between near-field modes during waveguiding, and a change in the far-field (free-space) divergence of the beam, after penetration through the etched foil. We show that the effects of dispersion and scattering may be studied optically from measurements of the spatial coherence of the pulses after travelling through the channel.

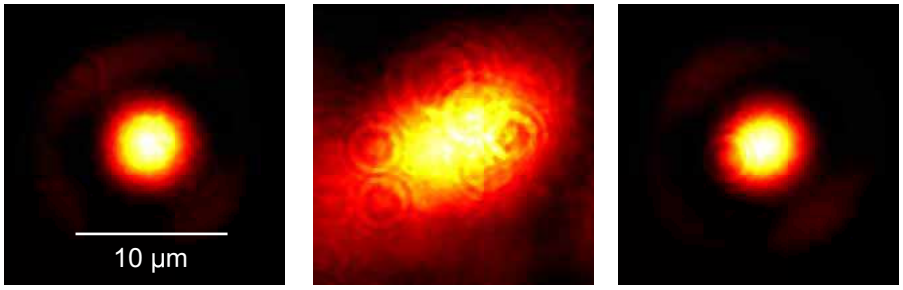

Fig. 2. (Color online) Left: Unobstructed beam-waist. Middle: Free-space propagation 150 μm past the unobstructed beam-waist. Right: Same as middle, but after drilling through 150 μm Al foil instead of free-space propagation. 1ps pulses in 133MHz pulsetrain-bursts, as described in experimental setup; same scale in all images.

For this study, we drilled channels through various thicknesses of aluminium foil, using pulsetrain-bursts of ultrashort laser pulses. Immediately after penetration, the transverse coherence and the beam profile were measured at the exit of the channel, together with incident and transmitted powers. These measurements and subsequent analysis were then used to understand how propagation changes the beam characteristics, and the resultant magnitude of this effect on the etch-rate reduction problem.

2. Experimental setup

We used a flashlamp-pumped Nd:glass system ($\lambda = 1054\,nm$), purpose-built at the University of Toronto [22]. This laser system was originally designed for single-pulse high-field experiments, selecting and amplifying a single 1-10ps pulse, but its oscillator allows for pulsetrain-bursts ($0.5 - 20\ \mu s$) at 133MHz repetition rate. This feature was used in this experiment, where we select a burst of pulses from the oscillator train for amplification and target interaction.

For this study, the near-circularly polarized beam was focussed to a spot size of 4 μm (FWHM) onto the front surface of aluminum foils using a 13.8mm-focal-length aspherical lens. The focus was regularly monitored by autocollimating the retroreflected beam, from which an equivalent-target-plane (ETP) image was recorded for each shot (Fig. 3). Each shot (or pulsetrain) was focussed onto the front surface of the foil, and the focus was not moved over the course of the pulsetrain. Temporal profiles and total energies of the pulsetrains were measured for incident and transmitted beams. A near-field image corresponding to the back surface of the target was captured to measure the beam size exiting the channel. A far-field image (25 mm after the target) was also recorded for future analysis involving after-target beamspread.

The length of the pulsetrain-burst, selected using a Pockels cell N-pulse slicer, was set such that only $0.5 - 1.5\ \mu s$ of pulsetrain passes through the dynamic channel after foil-penetration. This enabled us to optically characterize the pulses under the conditions of a channel during drilling, including effects of plasma, by analyzing only those pulses transmitted immediately after the target has been fully penetrated. This was done for different foil thicknesses from 25–150 μm. The energy incident on the target was adjustable up to $\sim 10\ \mu$J/pulse, giving a

#96527 - $15.00 USD Received 3 Jun 2008; revised 30 Jul 2008; accepted 17 Aug 2008; published 20 Aug 2008

total train energy of up to 12 mJ in a $10\mu s$ burst. The incident intensity was chosen to be 120% of the minimum value necessary for any length of pulsetrain to penetrate a given foil-thickness. Below this minimum, the intensity delivered at the end of the deep channel would drop below etch-threshold, and a complete channel would not form. In the typical case of 100 μm foil, the burst length was set to 7 μs (about 900 pulses), and the energy set to ~ 0.9 μJ/pulse, giving a total train energy of ~ 800 μJ, or total fluence of $\sim 6\ kJ/cm^2$ with a peak intensity of $\sim 6 \times 10^{12}$ W/cm^2.

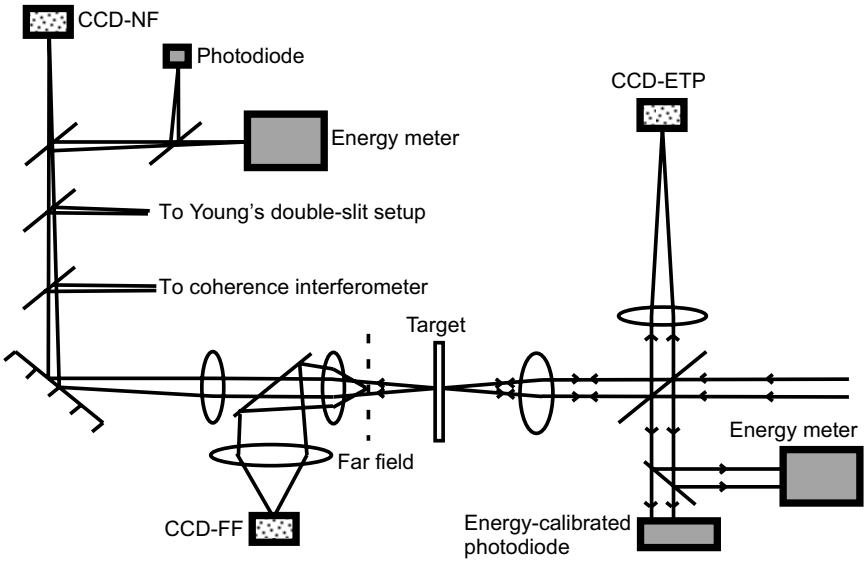

Fig. 3. Schematic of equivalent-target-plane (ETP), near-field (NF), and far-field (FF) imaging. The image of the exit aperture of the foil is relayed to the double-slit of Young's apparatus and also to the CCD plane of the coherence interferometer. Incident and transmitted energy and power were also recorded.

To measure the spatial coherence, Young's double-slit method was found to be unsuitable. To characterize the spatial coherence from a series of individual transverse separations would require many shots with many different slit separations. Instead, a folded-interferometer-based scheme was used to measure the transverse coherence in a single shot [23]. This involved interfering one instance of the near-field image with a copy which had been flipped left-to-right. The resulting interference pattern was recorded, as well as images of each component separately. From these, it was possible to measure the degree of spatial coherence as a function of transverse separation for all vertical positions of the beam, for each individual shot (Fig. 4).

3. Coherence analysis

From a map of the degree of spatial coherence as a function of horizontal separation and vertical position, it is convenient to consider only the vertical position corresponding to the middle height of the beam. This gives the degree of spatial coherence as a function of transverse separation over the brightest part of the beam [23]. Several of these have been plotted together in Fig. 5. This comparison shows that the interferometer-based scheme is in agreement with measurements made using Young's double-slit approach. It also directly shows that the process of drilling reduces the spatial coherence compared to free-space propagation.

To determine the transverse coherence of the transmitted light, the width (FWHM) of each

#96527 - $15.00 USD Received 3 Jun 2008; revised 30 Jul 2008; accepted 17 Aug 2008; published 20 Aug 2008

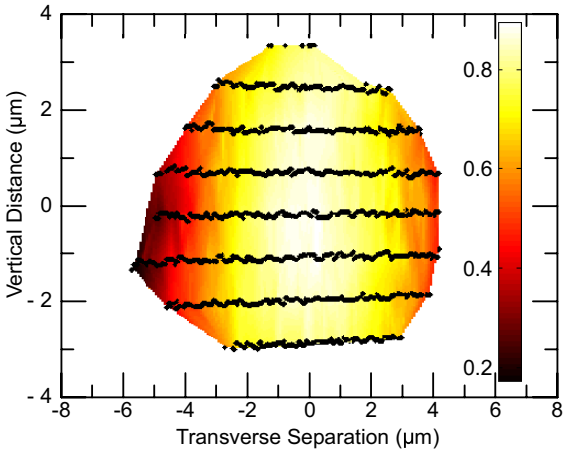

Fig. 4. (Color online) Map of degree of coherence as a function of transverse separation (x-axis) and vertical position (y-axis). The black dots correspond to fringes, where the coherence was measured. The colours (shades) indicate the calculated degree of coherence. Degree of coherence/fringe-visibility should go to 1 for zero-value separation; light-scattering and non-parallel beam geometry account for the defect. Interpolation between data-points was done by Delaunay triangulation.

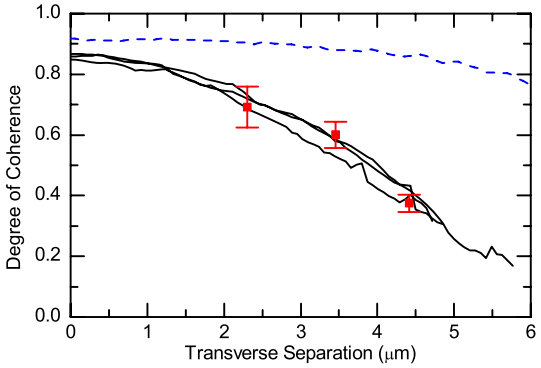

Fig. 5. (Color online) Degree of coherence *vs*. transverse separation. Solid (black) lines: drilling through 150μm of aluminium, measured using the interferometer. Discrete points: drilling through 150μm of aluminium, measured using Young's double-slit setup. Dashed (blue) line: free-propagated beam, measured using the interferometer. Each interferometer curve was obtained with a different single shot, and each double-slit point was obtained by averaging data over several shots.

degree-of-coherence curve was obtained. However, the width of the exit-beam itself varied by as much as 20% from shot to shot depending on the thickness of the foil. Therefore, the ratio of the spatial coherence length to the measured spot size was used for further analysis as described below. This was determined for each shot through various foil thicknesses (Fig. 6). These results show that this *degree of global coherence* drops as the pulses drill deeper into the foil.

In most cases, the near-field image (back surface of the foil) was approximately Gaussian, but showed an Airy-like ring (Fig. 2). The intensity of this secondary maximum varied from 10-20% of the peak intensity, and was ignored in all measurements.

#96527 - $15.00 USD Received 3 Jun 2008; revised 30 Jul 2008; accepted 17 Aug 2008; published 20 Aug 2008

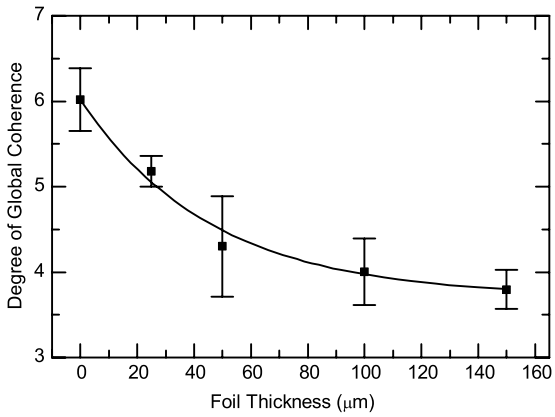

Fig. 6. Degree of global coherence *vs*. foil thickness. Each point corresponds to the mean of several measurements, and the error bars represent the standard error of the mean. The data is fit to an exponential curve.

4. Gaussian Schell-model

Standard Gaussian beam propagation theory applies only to completely spatially coherent sources, and is therefore not sufficient to describe a beam of limited degree of transverse coherence. A well-established theoretical model of sources with reduced spatial coherence is the Schell-model, which describes sources characterized by the property that the spatial correlation function of two points in a transverse plane depends only on their separation. This model has been extended to sources whose intensity distribution is Gaussian, and degree of coherence as a function of spatial separation is also Gaussian. This is referred to as a Gaussian Schell-model source [24]. The use of the Gaussian Schell-model to interpret our experimental findings is justified since our near-field images as well as the transverse coherence profiles are both approximately Gaussian distributions (Fig. 5). To arrive at a measure of the global coherence of a beam, we have to look at the interplay between the beam size and coherence length of the beam.

The radius of a beam generated by a Gaussian Schell-model source propagates as:

$$\rho_s(z) = \rho_s(0)\left\{1+\frac{z^2}{k^2\rho_s^4(0)}\left[1+4\left(\frac{\sigma_s}{\sigma_g}\right)^2\right]\right\}^{1/2} \tag{1}$$

The notation used is the same as that used by Mandel and Wolf [24]; the beam radius $\rho_s(z)$ at the propagated distance z is defined as the value at 1/e of maximum intensity. The wavenumber k is defined as usual. For the coherence width, $\rho_\mu(z)$, a similar expansion holds. The positive parameters σ_g and σ_s denote the state of coherence and the intensity distribution respectively, which are both suitably normalized:

$$\sigma_{s,g} = \frac{\rho_{s,\mu}(0)}{\sqrt{2}} \tag{2}$$

The ratio of the coherence width to the beam radius in a given transverse cross section defines the desired degree of global coherence, q.

$$q = \frac{\sigma_g}{\sigma_s} = \frac{\rho_\mu(z)}{\rho_s(z)} \tag{3}$$

#96527 - $15.00 USD Received 3 Jun 2008; revised 30 Jul 2008; accepted 17 Aug 2008; published 20 Aug 2008

This is invariant as the beam propagates. We note that in the spatially coherent limit ($\sigma_g \rightarrow \infty$), Eq. (1) reduces to the familiar Gaussian-beam propagation formula; as the spatial coherence decreases, the divergence of the beam increases.

5. Applying the Gaussian Schell-model

In free space, loss of transverse coherence translates into faster spreading of the spot-size with distance, relative to an idealized Gaussian model. In a laser-etched channel, with plasma at the irregular channel-walls, the pulses are waveguided by the boundary conditions at the plasma 'cladding', where the index of refraction is less than unity. Degradation of the transverse coherence in the near-field, concomitant with increased far-field divergence angle, can be expected to lead to coupling into leaky modes from which more energy will couple optically into the plasma, and from there by thermal conduction to the channel walls. This will reduce the optical intensity and etch-rate at the end of the channel, and aggravate the problem of etch-depth saturation in these channels.

The analogy with launch into a single-mode optical fiber is useful: a gaussian beam incident with the correct numerical aperture, or f-number, will couple energy into a trapped propagating mode, while a larger angle will couple energy to leaky modes which attenuate with distance. At the end of a long single-mode fiber, only light in the trapped mode will remain, which will output into a far-field angle corresponding to the acceptance angle of the propagating mode. Suppose now that a pulse of the proper acceptance angle is launched into the fiber, and trapped, but that phase-scattering during propagation degrades the transverse coherence of the pulse. The amplitude distribution of the near-field may be unaffected for the moment, but due to changes in the phase-distribution it will analyze differently over modes of the fiber. In free space, the waveform would propagate in the geometrical limit to a divergence angle larger than the fiber's acceptance angle; within the waveguide, it will partition energy to leaky modes which will attenuate, eventually reducing the on-axis intensity and effectively spatial-filtering the perturbed distribution.

The acceptance angle picture may similarly be applied to the pulses propagating in a laser-etched channel; roughly speaking, the profile and density of plasma at the channel walls determine a trapping condition for propagated light. Phase changes from surface irregularities and absorption in the plasma continually degrade the transverse coherence during propagation, and the perturbed distribution couples to leaky modes and is dissipated at the sidewalls at an enhanced rate.

The Gaussian Schell-model propagation formulae permit us to project our measured degradation of transverse coherence, taken from a series of near-field distributions at progressive etch-depths, into the equivalent free-propagation far-field divergence. This gives a metric of the propagating beam, which when compared to an effective 'acceptance angle' parameter would characterize the degree of trapping.

Direct calculation of trapping in the waveguide is complicated, since the plasma index-of-refraction is complex-valued due to collisions, and since the thickness and profile of the plasma layer are virtually unaccessible, experimentally. The output far-field divergence does not characterize the trapping condition, since degradation of spatial coherence is continuous, and it is unlikely that leaky modes attenuate fully over our relatively short distances. Numerical simulation will be useful, qualitatively, but may not predict conditions with sufficient definiteness to add quantitative information.

Absent a definitive effective acceptance angle, and for our propagation over just a few Rayleigh ranges, we have simply estimated propagation losses by using the Gaussian Schell-model, and our measured degrees of global coherence, to project an effective perturbed mode-size onto a characteristic exit aperture for the channel. The same calculation for pure Gaussian

#96527 - $15.00 USD Received 3 Jun 2008; revised 30 Jul 2008; accepted 17 Aug 2008; published 20 Aug 2008

propagation permits a comparison that makes clear the impact of degraded spatial coherence.

For the Gaussian Schell-model, the redistributed laser energy remaining within an exit-disk of radius a was calculated. When this energy is normalized to the total energy, this gives a transmission T which depends on the thickness of the foil z:

$$T = 1 - exp\left\{\frac{-a^2}{\rho_s^2(0)\left[1+\frac{z^2}{k^2\rho_s^4(0)}\left(1+\frac{4}{q}\right)\right]}\right\} \tag{4}$$

The pure-Gaussian case can be recovered by the assumption of perfect spatial coherence, *i.e.*, $q \rightarrow \infty$.

This propagated transmission can also be inferred empirically by measuring the energy of pulses transmitted through the foils, immediately after the foils are pierced. We compare the empirical and expected intensities by comparing the energy-transmission efficiency for different foil-thicknesses.

For our calculations, the size of the beam at the entrance of the channel was measured directly (using no target), and the degree of global coherence was then measured for the transmitted light on each shot through foils of different thicknesses. Gaussian Schell-model propagation formulae were used to calculate the intensity distribution of an equivalent freely-propagating beam (*i.e.*, having this measured beam-waist and degree of global coherence) at a distance from the beam-waist corresponding to the thickness of the foil. The size of our effective exit-aperture was approximated as $4\times$ the FWHM spot size. This size is approximately equal to the diameter of the beam obtained from the outer radius of the near-field Airy-like ring (Fig. 2).

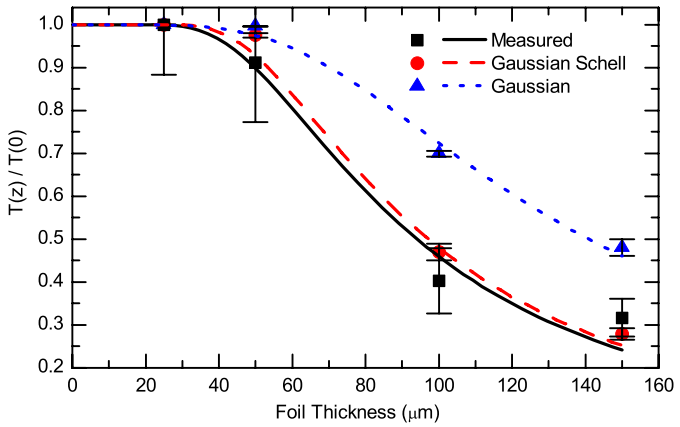

Fig. 7. (Color online) Normalized transmission *vs*. foil thickness: experimental transmission (squares) compared to values expected under Gaussian (triangles), and Gaussian Schell-model (circles) propagation. Expected values are calculated from measured coherence at each foil thickness, and include error-bars. Each set of data is fit by a curve of the form of Eq. (4), to illustrate the trends.

The impact of degraded transverse coherence during channel-etching shows directly, in the comparison of the experimentally measured transmission to that expected as above by Gaussian and by Gaussian Schell-model propagation (Fig. 7), for foils of increasing thickness. According to both the Gaussian and Gaussian Schell-models, the transmission through $25\mu m$ foil is over 0.99, so this may be treated as an essentially thin foil. The measured transmission however, is only 0.18, indicating that approximately 80% of the energy is lost due to back-scattering and

#96527 - $15.00 USD Received 3 Jun 2008; revised 30 Jul 2008; accepted 17 Aug 2008; published 20 Aug 2008

coupling efficiency regardless of channel depth. To compare only propagation effects in Fig. 7, transmission is normalized to the zero-thickness value.

There is a significant dependence on the assumed value of the effective exit-aperture, but in all cases the inclusion of the observed degradation of transverse coherence more closely describes the experimental observation. The systematic loss of transverse coherence clearly makes an important and systematic contribution to the decay of etch-rate in these channels, and contributes to the ultimate depth a given set of laser parameters can produce.

6. Discussion

The physical picture we use here to describe the impact of degraded spatial coherence is qualitatively useful, but a host of physical subtleties will complicate a more quantitative description. In terms of waveguiding, it has been observed that when laser-drilling a channel, the channel usually gradually tapers with depth; the description of propagating and trapping modes is complicated by such geometries, unless the taper is slight and changes are essentially adiabatic. In our case, with plasma always present in the channel, it's unclear whether this effect contributes significantly during etching.

Large-scale boundary condition roughness would also complicate the waveguide description of laser-etched channels. Significant structures, especially immediately after the channel has been formed, have been observed [25, 26, 27], and could tend to scatter the pulses as they propagate down the channel. Plasma within the channel during etching may greatly reduce the impact of surface roughness; the self-consistent plasma profile may indeed assist waveguiding.

Most significantly, in calculating the intensity available for etching, after waveguide losses due to decreased spatial coherence, different leaky modes will dissipate at different rates dI/dz along the channel; the distinction of trapped modes and the definition of acceptance angle is not sharp, for the length-scales we consider. For this reason especially, though we show clearly an impact of degraded spatial coherence on etch-rate saturation, real quantification will require numerical simulation of the density and profile of plasma within the channel, and self-consistent calculation of the propagation of the etching laser pulses.

7. Conclusions

It is generally considered that absorption is the principal cause of reduced etch-rate in machining with ultrafast lasers. However, we have shown that purely optical propagation-effects need to be considered as well, especially when etching deep holes: for a pulse propagating down a long channel being etched, the waveguide structure and residual plasma impose significant changes on the internal phase relations of the pulses, and for deep channels optical effects could end up dominating the reduction of the intensity available for drilling.

We have directly measured the phenomenon of degradation of spatial coherence resulting from channel-etching. We have shown that this degraded spatial coherence acts to increase the divergence of the beam as it propagates through the channel, which will in turn affect waveguiding in the channel, energy absorption in the sidewalls, the delivered intensity and consequent etch-rate. The effect was illustrated, using a Gaussian Schell-model to connect our measured spatial coherence and measured beam-transmission at the exit-hole of our channels. The measured transmission was found to be in good agreement with that predicted using our model involving waveguiding with reduced spatial coherence.

Acknowledgments

The authors acknowledge support from the Canadian Institute for Photonic Innovations, the Centre for Photonics of Ontario Centres of Excellence, Inc., and the Natural Sciences and En-

#96527 - $15.00 USD Received 3 Jun 2008; revised 30 Jul 2008; accepted 17 Aug 2008; published 20 Aug 2008

gineering Research Council of Canada.

#96527 - $15.00 USD Received 3 Jun 2008; revised 30 Jul 2008; accepted 17 Aug 2008; published 20 Aug 2008